Rolled-Up Magnetic Sensor: Nanomembrane Architecture for In-Flow Detection of Magnetic Objects

Ingolf Mönch,[†,*] Denys Makarov,[*,†] Radinka Koseva,[†] Larysa Baraban,[†] Daniil Karnaushenko,[†,‡] Claudia Kaiser,[§] Karl-Friedrich Arndt,[§] and Oliver G. Schmidt[†,‡]

[†]Institute for Integrative Nanosciences, IFW Dresden, Helmholtzstrasse 20, 01069 Dresden, Germany, [‡]Material Systems for Nanoelectronics, Chemnitz University of Technology, Reichenhainer Strasse 70, 09107 Chemnitz, Germany, and [§]Physical Chemistry of Polymers, Dresden University of Technology, Mommsenstrasse 13, 01062 Dresden, Germany

ABSTRACT Detection and analysis of magnetic nanoobjects is a crucial task in modern diagnostic and therapeutic techniques applied to medicine and biology. Accomplishment of this task calls for the development and implementation of electronic elements directly in fluidic channels, which still remains an open and nontrivial issue. Here, we present a novel concept based on rolled-up nanotechnology for fabrication of multifunctional devices, which can be straightforwardly integrated into existing fluidic architectures. We apply strain engineering to roll-up a functional nanomembrane consisting of a magnetic sensor element based on $[Py/Cu]_{30}$ multilayers, revealing giant magnetoresistance (GMR). The comparison of the sensor's characteristics before and after the roll-up process is found to be similar, allowing for a reliable and predictable method to fabricate high-quality ultracompact GMR devices. The performance of the rolled-up magnetic sensor was optimized to achieve high sensitivity to weak magnetic fields. We demonstrate that the rolled-up tube itself can be efficiently used as a fluidic channel, while the integrated magnetic sensor provides an important functionality to detect and respond to a magnetic field. The performance of the rolled-up magnetic sensor for the in-flow detection of ferromagnetic CrO_2 nanoparticles embedded in a biocompatible polymeric hydrogel shell is highlighted.

KEYWORDS: rolled-up nanotechnology · rolled-up magnetic sensor · GMR sensor · fluidics · detection of magnetic particles · hydrogel

Modern diagnostic and therapeutic techniques, applied in medicine and biology, often rely on magnetic nanoparticles.[1−4] After careful studies of their properties[5−7] and biocompatibility,[8] magnetic particles have entered commercial applications, helping to detect proteins[9] and nucleic acids[10] or to enhance magnetic resonance imaging (MRI) contrast.[11] Currently, novel concepts for drug and gene delivery, based on magnetofection,[12] as well as magnetic cell sorting[13] are under development. As such, the need for integration of magnetic field sensing devices into biomedical systems is greatly increasing.

Previous efforts have mostly concentrated on static detection of magnetic nanoparticles placed in close vicinity of a magnetic sensor.[14,15] However, for high-throughput analysis of biochemical substances, fluids of complex media with different objects (*i.e.*, nanoparticles, living cells, droplets) have to be tested in a short time. There are two possible configurations for the development of an efficient magnetic biosensing platform: The first one is based on a movable giant magnetoresistance (GMR) sensor, referred to as a microplate reader,[16] which is rather expensive. An alternative solution is to perform the detection of magnetic particles in flow with a stationary magnetic sensor. Such microfluidic biosensors can provide high reproducibility and precise control over the injected chemical content and would be available at a low price. The approach to realize this concept is sketched in Figure 1a: Organic and/or inorganic objects possessing a permanent magnetic moment are detected and counted when they are traveling from an inlet reservoir through a fluidic channel to an outlet reservoir. A magnetic sensor device is integrated in the fluidic channel, and, whenever a magnetic object passes by, its magnetic stray field is detected electrically through a magnetoresistive effect. As the magnetic moment of the nanoobjects is rather small, the magnetic sensor device should be highly sensitive to small magnetic fields, which can be achieved by devices relying on the magnetoresistive effects and in particular on the GMR effect.[17−19] To this end, *planar* magnetic sensors were already incorporated in microfluidic channels, enabling dynamic detection of magnetic particles.[20,21]

Ultimately, a magnetic sensor element has to be directly integrated into a fluidic channel. In this respect, strain engineering[22,23] has already been proven to provide an elegant way to fabricate on-chip three-dimensional rolled-up architectures including optical

* Address corresponding to d.makarov@ifw-dresden.de, i.moench@ifw-dresden.de.

Received for review June 25, 2011 and accepted August 23, 2011.

Published online August 23, 2011
10.1021/nn202351j

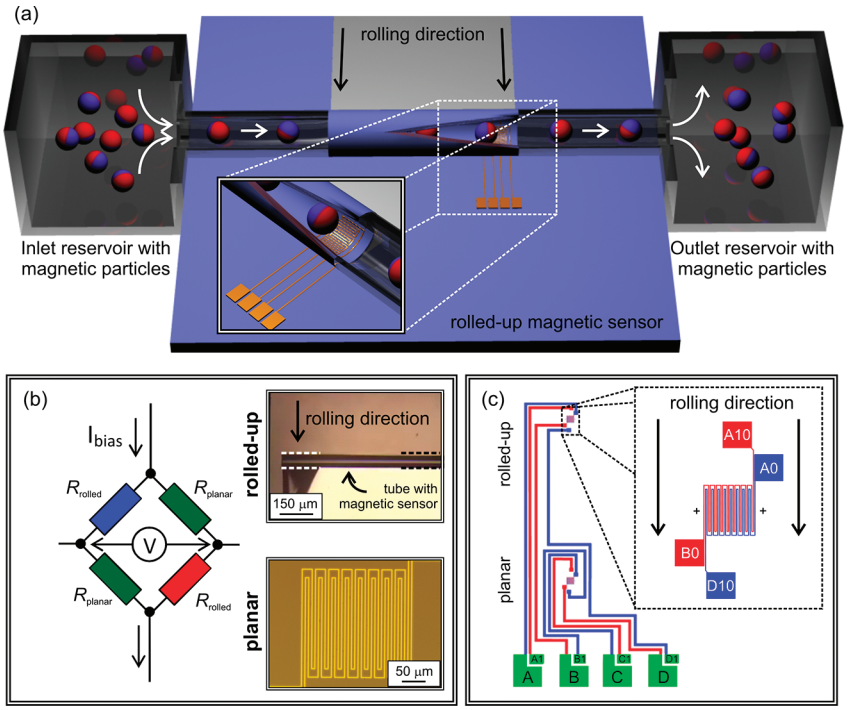

Figure 1. Basic concept and experimental realization. (a) Schematics revealing the main concept of rolled-up magnetic sensor for in-flow detection of magnetic objects: Magnetic objects in a fluidic channel can be easily detected and counted using the fully on-chip integrated rolled-up magnetic sensor. (b) Magnetic sensors are arranged in a bridge configuration to enhance the sensitivity of the device. The insets in (b) show the optical micrographs of the planar and rolled-up sensors. (c) Photolithographic mask used for the fabrication of the magnetic sensor elements in a bridge configuration. The individual magnetic sensor has a meander shape, as shown in the close-up image in panel (c). The rolling direction is indicated by arrows. Geometrical parameters of the realized sensors: the width of a single line in a meander is 4 μm. The length of the sensor in the direction of rolling is fixed to 200 μm. The number of periods in the meander structure was varied between 2.5 and 8.5, which in turn determines the total width of the sensor: 60 and 210 μm for the sensors with 2.5 and 8.5 periods, respectively. Panel (c) shows the mask to fabricate the meander with 8.5 periods. The total length of the rolled-up architecture is 15 mm; the diameter of the rolled-up tube including the GMR sensor is 60 μm.

resonators,[24,25] cell culture scaffolds,[26−29] compact electrical components,[30−32] optical fibers,[33] ferromagnetic microtubes[34] and microhelixes,[35] and liquid viscosity sensors[36] to name just a few. Rolled-up nanotechnology relies on the release of a strained nanomembrane on a sacrificial layer, leading to bending of the nanomembrane into a nano/microtube of customized size and geometry.

Here, we fabricate a fully integrative rolled-up GMR sensor simultaneously acting as a fluidic channel for in-flow detection of magnetic particles. The advantages of this device are intriguing: (i) the sensor covers part of the *inner* wall of the fluidic channel and as such is positioned in closest possible vicinity to the flowing objects. This particular geometry may lead to better signal-to-noise ratio of the device compared to the case when the sensor is positioned *outside* the channel. (ii) The rolled-up geometry makes the sensor sensitive to magnetic stray fields of the particles under study in virtually all directions. This avoids implementation of an external magnet to align the magnetic moment of the particle relative to the position of the sensor. Both these aspects are crucial for efficient and successful in-flow detection of magnetic objects.

RESULTS AND DISCUSSION

In this study, we arranged the magnetic sensors into a standard Wheatstone bridge configuration, as shown in Figure 1b. This scheme avoids constant bias voltage being applied to the measurement system and provides high differential sensitivity,[37] which is crucial when a small change in resistance needs to be detected. Furthermore, the bridge configuration provides good stability of the sensor's response against temperature changes. This is of great advantage, as the sensor can be used even when heating or cooling of the fluid is required, which is often the case when working with biological samples. The bridge arrangement requires fabrication of four independent resistors connected electrically pairwise (Figure 1b,c). Two of the four sensors are rolled-up into a tubular geometry, while the two other sensors remain planar and serve as reference for the electrical measurements (insets in Figure 1b). In order to increase the resistance, the sensors are meander-like shaped, as shown in the inset in Figure 1b. Meanders are photolithographically patterned using the mask shown in Figure 1c. The distance between the planar and rolled-up sensors is about 20 mm, which is sufficiently large to leave the planar ones

unaffected by applying an external magnetic field at the location of the rolled-up sensors. The complete device in planar arrangement before the rolling process is shown in Figure 2a. In order to capture all peculiarities of the device using the same camera magnification, the layout with a rather large sensor area of 1 × 1 mm^2 was chosen in contrast to the device with a sensor area of 200 × 60 μm^2 used for the purpose of this work (see discussion below).

In order to fabricate tube-like magnetic sensors, we rely on rolled-up nanotechnology[22,38] employing photoresist as sacrificial layer.[39−41] On thermally oxidized Si(100) wafers, a polymeric sacrificial layer (resist ARP 3510) was deposited on a locally defined area. Next, an auxiliary layer for roll-up consisting of a 100-nm-thick CuNiMn alloy film was prepared. A 20-nm-thick electrically isolating Al_2O_3 layer was introduced prior to and after deposition of the GMR stack consisting of Py(1.5 nm)/[Py(1.5 nm)/Cu(2 nm)]$_{30}$ multilayers. The complete layer stack is schematized in Figure 2b. The thicknesses of the individual Py and Cu layers in the GMR stack were optimized to achieve [Py/Cu]$_{30}$ multilayers coupled in the second antiferromagnetic maximum. The latter allows enhancing the sensitivity of the sensor in the low-field region,[17] thus representing a good compromise between high sensitivity and sufficiently high GMR ratio. In this way, a GMR ratio of about 6.5% was measured for the planar sensor (Figure 3a), with a sensitivity as high as 2.8 Ω/mT (1.4%/mT) in the field of 1.4 mT (Figure 3b). The GMR ratio is defined as the magnetic field dependent change of the sample's resistance, $R(H)$, normalized to the value of resistance when the sample is magnetically saturated, R_{sat}: GMR(H) = [$R(H) - R_{sat}$]/R_{sat}; H is an external magnetic field. Furthermore, the sensitivity of the sensor element is defined as the first derivative of the sample's resistance over the magnetic field: $S(H) = dR(H)/dH$. The measured value of the GMR of about 6.5% is only slightly smaller than that achieved for the planar sensor based on the tunneling magnetoresistive (TMR) effect built in the fluidic channel.[20]

After deposition of the GMR multilayer stacks, photolithography and wet-chemical etching of the metal films was performed in order to define the meander-like shape of the sensors and the electrical contacts (Figure 2a). The width of a single line in a meander is 4 μm. The length of the sensor in the direction of rolling is 200 μm. The number of periods in the meander structure was varied between 2.5 and 8.5, which in turn determines the total width of the sensor: 60 and 210 μm for the sensors with 2.5 and 8.5 periods, respectively. The width of the sensor has to be optimized to the size of the magnetic object under consideration. Thus, for the particles of choice with diameters of 40 μm, the number of windings in the GMR meander was fixed to 2.5. The roll-up procedure was performed in acetone under microscopic observation.

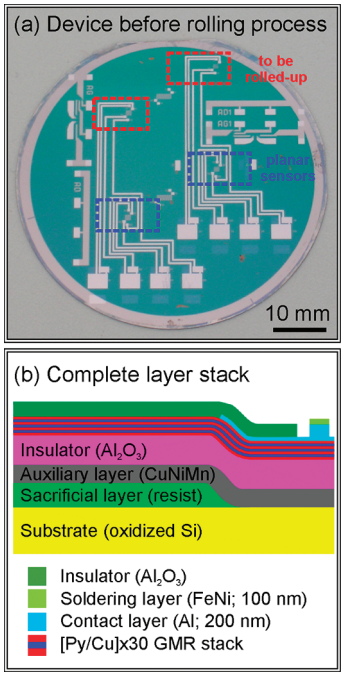

Figure 2. (a) Photograph of the complete device in planar arrangement before rolling process. The layout with a sensor area of 1 × 1 mm^2 is shown. Please note that the device with a sensor area of 200 × 60 μm^2 was used for the purpose of magnetic particle detection. (b) Schematics of the layer stack.

The total length of the rolled-up architecture is 15 mm; the diameter of the rolled-up tube including the GMR sensor is 60 μm. Given that the length of the sensor in the rolling direction is 200 μm, this results in a single winding of the sensor in the rolled-up tube with multiple windings. Using a CuNiMn auxiliary layer, rolled-up architectures with diameters from 15 to 60 μm can be achieved.[40]

Figure 3 shows the magnetoresistive performance (GMR ratio and sensitivity) measured at room temperature for a single meander-shaped [Py/Cu]$_{30}$ multilayer before and after the roll-up process. The magnetic field was applied in the substrate plane along the axis of the rolled-up tube. Details on electric connections are given in the Methods section. The GMR ratio measured for the rolled-up sensor is found to be only slightly smaller than for the planar counterpart (Figure 3a). Even more important, the sensitivity of the rolled-up sensor in the low-field region is comparable to the one measured for the planar sensor (Figure 3b). The optimum performance of the *rolled-up sensor* with respect to its sensitivity of about 2.6 Ω/mT (2.3%/mT) is achieved in magnetic fields of about 1.4 mT. The typical sensitivity for the *planar* TMR-based sensors in the low-field region (~1.5 mT) is about 4%/mT,[20] which is only slightly better than the sensitivity of the *rolled-up* GMR sensor (2.3%/mT) measured in the present work. This sensitivity results in voltages in the range of 5 mV to be detected by passing current of 2 mA. This voltage is easy to detect using any conventional multimeter

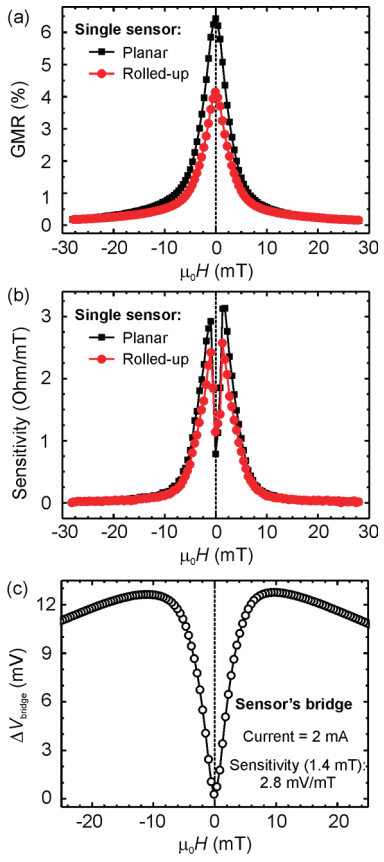

Figure 3. GMR performance of the magnetic sensor. (a) Response of the GMR meander to an external magnetic field measured using planar (squares) and rolled-up (circles) structures. The GMR performance of the rolled-up magnetic sensor is only about 2% lower than the planar sensor. Resistance at zero magnetic field is 260 Ω (rolled-up sensor) and 210 Ω (planar sensor). (b) Sensitivity of the planar (squares) and rolled-up (circles) sensor elements. (c) Change of bridge voltage measured as a function of an external magnetic field for the two rolled-up and two planar GMR sensors connected in a bridge configuration. The sensitivity of the bridge is 2.8 mV/mT when measured at about 1.4 mT.

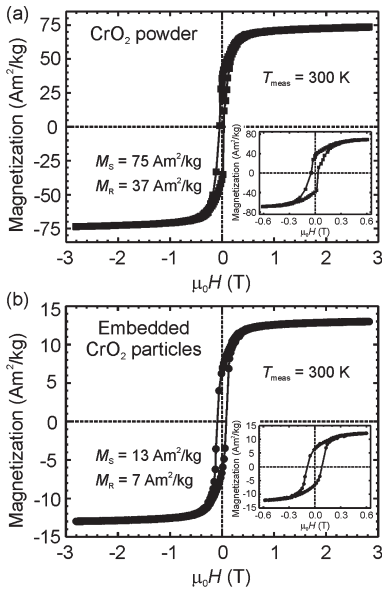

Figure 4. Magnetic characterization of the CrO_2 powder samples: Magnetic hysteresis loops measured at 300 K of the (a) CrO_2 powder and (b) embedded CrO_2 nanoparticles into a polymeric hydrogel shell with a diameter of 40 μm. Magnetic nanoparticles are evenly distributed in the polymer. The size of an individual CrO_2 nanoparticle is about 300 × 30 nm². The size of the resulting object used for the in-flow detection is about 40 μm. Although a certain fraction of CrO_2 nanoparticles is superparamagnetic, the magnetic moment at remanence, M_R, is sufficiently high to be detected with the rolled-up magnetic sensor.

without special equipment or signal enhancement procedures.

The detection of magnetic particles is carried out using the rolled-up GMR sensor as part of the bridge configuration. The response of the sensor bridge to the external magnetic field occurring locally at the two rolled-up sensors is shown in Figure 3c. Please note that only the difference between the bridge voltages measured when a magnetic field is applied and without magnetic field is plotted. When measured in the bridge configuration, only two rolled-up meanders were exposed to the magnetic field. Two planar sensors were outside of the electromagnet, which is easily realizable, as the distance between planar and rolled-up sensors is 20 mm (Figure 2a).

The performance of the sensor was investigated for in-flow detection of magnetic CrO_2 nanoparticles (Magtrieve) encapsulated into a polymeric hydrogel shell (about 8 wt % of CrO_2) with an average diameter of about 40 μm. The polymer shell of such magnetic capsules is easy to functionalize and highly biocompatible. The size of the CrO_2 is about 300 × 30 nm².[42] The particles are sufficiently large to be ferromagnetic, with the easy magnetization axis of the individual particles pointing along their long axis. Magnetic characterization of the as-prepared CrO_2 powder carried out at room temperature using vibrating sample magnetometry (VSM) revealed the nonzero remanence and coercive field, which proves that at least part of the sample is ferromagnetic. However, the characteristic S-like shape of the hysteresis loop (Figure 4a) suggests that there is a superparamagnetic contribution to the signal as well. The saturation magnetization, M_S, of the CrO_2 powder is about 75 Am²/kg, which is in agreement with previously published data.[42,43] Embedded CrO_2 particles in a hydrogel shell are subject to a more pronounced magnetic hysteresis (Figure 4b) with larger coercive field compared to the as-prepared CrO_2 powder. Hysteresis loops measured at room temperature for the as-prepared CrO_2 powder as well as for the embedded CrO_2 nanoparticles reveal a remanent magnetization of about 0.5 (normalized to the saturation magnetization), which is typical for the assembly of the Stoner–Wohlfarth particles with randomly distributed easy axes of magnetization.[44] Although the saturation magnetization of the embedded CrO_2 particles is about 13 Am²/kg, the remanence magnetization is still

sufficiently high to be detected by the rolled-up GMR sensor.

As a reference measurement we placed a single object containing CrO_2 nanoparticles on the planar GMR meanders, and a difference of the bridge voltage of 10 mV was detected (not shown). This signal is substantially stronger and thus easier to measure, compared to literature results of about 80 μV measured for the planar TMR sensor built in the fluidic channel.[20] However, the particles investigated in ref 20 had a size of only 2.8 μm. Furthermore, the signal-to-noise ratio determined for the measurement using *planar GMR meanders* in the bridge is 46 dB (10 mV signal; 0.05 mV noise), which is higher compared to the 24 dB measured for the planar TMR sensor.[20]

The dynamic measurement of the magnetic particles passing through the microfluidic channel in the vicinity of the GMR sensor is shown in Figure 5. The microfluidic circuit was designed to realize dynamic in-flow detection of magnetic CrO_2 nanoparticles embedded in a hydrogel shell. This circuit consists of the inlet for injection of the solvent containing the beads, the rolled-up tube as a fluidic channel equipped with the GMR sensor, and the outlet to collect the utilized solution. The hydrogel beads with an average diameter of 40 $\pm$ 10 μm containing randomly distributed elliptical CrO_2 nanoparticles were dispersed in organic solvent (toluol). As the size of the hydrogel beads is only slightly smaller than the diameter of the rolled-up tube (60 μm), only single magnetic objects fit through the rolled-up GMR channel. The external magnetic field was switched off during particle detection. Sparsely distributed magnetic beads were moved through the channel with a constant velocity of about 1 mm/s. When the magnetic hydrogel beads reach the detection area of the rolled-up sensor, the voltage measured between the sensing electrodes, ΔV_{bridge}, changes and only drops back to its original value once the magnetic objects have left the vicinity of the sensor. The response of the sensor is reliable with an average amplitude of 9 mV (Figure 5). By recording the sensor's output voltage, every single hydrogel bead with the encapsulated magnetic nanoparticles is clearly resolved and can easily be counted. The signal-to-noise ratio determined for the measurement using *rolled-up GMR meanders* in the bridge is 45 dB (9 mV signal; 0.05 mV noise). The negative peak at about 110 s (Figure 5) is an artifact of the measurement, which *might* be related to a shortcut through the Al_2O_3 isolating layer during filling the rolled-up channel with fluid. The shift of the baseline right after the negative peak is then due to the relaxation of the channel to its initial diameter and slow "healing" of defects in the isolation layer. For the purpose of the work, several independently prepared devices were tested, always providing reliable response, similar to the one shown in Figure 5.

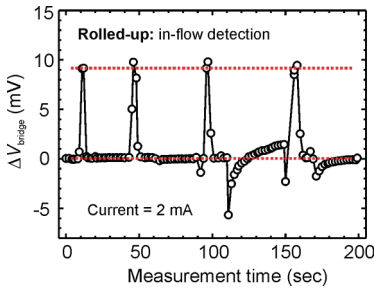

Figure 5. Magnetic particle detection. Time evolution of the bridge voltage measured while magnetic particles pass the rolled-up sensor. Please note that the difference of the bridge voltage of 10 mV was detected if a single bead with CrO_2 nanoparticles was placed on a planar GMR meander.

CONCLUSION

In conclusion, we have developed rolled-up magnetic sensor devices that rely on the giant magnetoresistance effect of magnetic $[Py/Cu]_{30}$ multilayers. A couple of steps were undertaken to enhance the sensitivity of the magnetic sensor for in-flow detection of magnetic objects in fluidic channels: (i) the GMR multilayers were coupled in the second antiferromagnetic maximum, providing high sensitivity to low magnetic fields, and (ii) the sensors were arranged in a Wheatstone bridge configuration, allowing for improved differential sensitivity. We measured the response of the rolled-up GMR sensor to stray fields of magnetic particles passing through a microfluidic channel defined by the rolled-up device itself. This approach might be beneficial for efficient biodetection of protein structures,[9] diagnostics of diseases,[45] and sorting of living cells.[46] The advantage of rolled-up devices is their straightforward integrability into existing on-chip technologies and the ability to combine several functions into a single architecture, possibly leading to a fully operational lab-in-a-tube system.[29,40]

METHODS

Fabrication of the Rolled-Up GMR Sensor. For sample preparation a standard class 100 clean room equipped with a broad spectrum of technological tools for thin film preparation was used. On thermally oxidized Si(100) wafers with contacts and chip numeration, a polymeric sacrificial layer was deposited on a locally defined area. For the sacrificial layer the resist ARP 3510 (the Allresist GmbH, Strausberg, Germany) was applied. An auxiliary roll-up layer consisting of a 100-nm-thick CuNiMn alloy film was deposited by magnetron sputter deposition at room temperature. The lateral geometry was defined using optical lithography and selective wet-chemical etching. The etching process was carried out at room temperature in a Fe_3Cl basis solution. A 20-nm-thick electrically isolating Al_2O_3 layer was

introduced prior to deposition of the GMR stack consisting of Py(1.5 nm)/[Py(1.5 nm)/Cu(2 nm)]$_{30}$ multilayers. A second Al_2O_3 isolating layer is applied to electrically decouple the GMR sensor layer for application in the fluidic environment. Atomic layer deposition was used to fabricate Al_2O_3 films, which provide very dense isolating films at low thickness (down to 5 nm) at a relatively low deposition temperature of about 90 °C. The low temperature is important if photoresists are used as a sacrificial layer for the roll-up process. Prior to electrical studies, we checked the insulating performance of the Al_2O_3 layer by determining the breakthrough field strength. The breakthrough field was measured in tunnelling geometry and determined at the voltage where a critical current density of 0.1 μA/cm^2 was exceeded. After deposition of the GMR multilayer stacks, photolithography (or electron beam lithography) and chemical etching of the metal films were performed in order to define the meander-like shape of the sensors and define electrical contacts. These structures were rolled up with widths ranging from 100 nm up to 50 μm. A length to width ratio of the sensor from 2 to 2000 was achieved, allowing careful adjustment of the sensor dimensions to the size of an object that needs to be detected. For the scope of the present study, we optimized the dimensions of the sensor to a size of 40 μm: number of periods in GMR meander is 2.5; sensor width is 4 μm; sensor area is 200 $\times$ 60 μm^2. Furthermore, the maximal size of the GMR meander of 1 $\times$ 1 mm^2 was fabricated. This sensor arrangement is presented in Figure 2a. The patterning processes were carried out by means of the lift-off technique as well as by chemical and physical etching. The roll-up procedure was performed in acetone under microscopic observation. For the drying procedure a critical point dryer, CPD 030 (Bal-Tec, Liechtenstein), was used to avoid the collapse of the tube structures.

Preparation of [Py/Cu]$_{30}$ GMR Multialyers. This step includes magnetron sputter deposition at room temperature of Py(1.5 nm)/[Py(1.5 nm)/Cu(2 nm)]$_{30}$ multilayer stacks exhibiting GMR effect. Deposition conditions are as follows: base pressure 7.0 $\times$ 10^{-7} mbar; Ar sputter pressure 7.5 $\times$ 10^{-4} mbar; deposition rate 2 Å/s. The thickness of individual Py and Cu layers was optimized in order to achieve Py/Cu multilayers coupled in the second antiferromagnetic maximum.

Electrical Characterization and Temperature Stability of the GMR Meander. The electrical characterization was carried out at room temperature using a four-point resistance measurement on subμm prober PSM 6 by applying the source unit Keithley 236 and the nanovoltmeter Keithley 182. For the measurement of a single planar and rolled-up meander, a four-point measurement scheme was used. The contacts used are color-coded in Figure 1c. In particular, two blue-indicated contacts were used to measure voltage (pads A0 and D10) and send current (pads A and D1) to the rolled-up meander. Measurements on the bridge were performed in the bridge configuration shown in Figure 1b. In order to do this, two pairs of contacts for example contact pads D and D1 in Figure 1c were connected by bonding using ultrasonic wire bonding (setup DELVOTEC 5425).

When current flows through the meander, a circular magnetic field is induced. This field might influence the resistance of the second (neighboring) meander. However, as this current is only 2 mA, the magnetic field is not strong to influence substantially the neighboring GMR meander. Such measurement was carried out, and the relative change of below 0.005% of the meander's resistance was measured. This is substantially smaller compared to the relative resistance change while detecting magnetic particles.

The temperature stability measurement was carried out in the temperature range 20 °C < T < 130 °C. The setup is equipped with an electromagnet providing a magnetic field of about 80 mT. The temperature coefficient of the GMR [Py/Cu]$_{30}$ multilayer stack was measured to be 1440 ppm/K. Therefore, stabilization of the temperature drift of the sensor's resistance for precise detection of small magnetic signals becomes crucial. This thermal stability is achieved by contacting GMR sensors in a standard Wheatstone bridge configuration (Figure 1b,c).

Synthesis of Magnetic Microgels. Temperature-sensitive hydroxypropyl cellulose (HPC) hydrogels undergo reversible volume transitions between 40 and 45 °C. The HPC were purchased from Aldrich Chemical Co. and used as received. The molecular weight of the HPC (M_w = 100.000 g/mol) was determined by static light scattering in ethanol (SLS Systemtechnik G. Bauer, Freiburg, Germany). The glass transition temperature was 196 °C (DSC 2920 CE, TA Instruments GmbH, nitrogen, temperature range −50 to 350 °C, heating rate 5 K per minute). Divinyl sulfone (DVS, Aldrich Chemical Co.) was used as cross-linker, and chromium dioxide (Magtrieve, Aldrich Chemical Co.) as filling material. The hydrogels for further experiments were synthesized as cylindrical gels (diameter of about 0.5 cm) according to the procedure described by Harsh *et al.*[47] HPC (7.5 g) was dissolved in 0.05 M KOH (92.5 mL) and mixed with 73 wt % nanoparticles (in relation to the initial weight of HPC). The suspension was homogenized in an ultrasonic bath for 10 min. After adding the DVS (1 mL) the solution was shaken and poured in plastic tubes that are closed at both ends. To prevent sedimentation of the filler, the plastic tubes were rotated during the cross-linking reaction (72 h at room temperature). The gels were extracted for another 72 h in deionized water (changing water after every 6 h). The cylindrical gels were used powdered, so they have to be dried for 7 days at room temperature under vacuum. Preparation of the polymer shells containing magnetic nanoparticles includes cooling the gel material to −78 °C (using dry ice). Next, mechanical milling was applied followed by separation of functionalized particles according to their diameter. In order to do so, sieves with different mesh sizes of 125, 100, 90, 75, 60, 40, and 20 μm were applied. For the purpose of the present work, particles were selected using sieves with a mesh size of 40 and 60 μm.

Acknowledgment. The authors acknowledge valuable discussions with R. Kaltofen, M. Melzer, and Dr. S. Sanchez. We thank I. Fiering for the assistance in the deposition of the magnetic layers. This work is financed in part *via* the German Science Foundation (DFG) grants MO887/1-2, AR193/11-2, priority program SPP 1259, Volkswagen Foundation (I/84 072), and DFG Research Unit 1713 "Sensoric Micro- and Nanosystems".

REFERENCES AND NOTES

1. Salata, O. V. Applications of Nanoparticles in Biology and Medicine. *J. Nanobiotechnol.* **2004**, *2*, 3.
2. Mönch, J. I.; Meye, A.; Leonhardt, A.; Krämer, K.; Kozhuharova, R.; Gemming, T.; Wirth, M. P.; Büchner, B. Ferromagnetic Filled Carbon Nanotubes and Nanoparticles: Synthesis and Lipid-Mediated Delivery into Human Tumor Cells. *J. Magn. Magn. Mater.* **2005**, *290*−*291*, 276–278.
3. Reddy, S. T.; van der Vlies, A. J.; Simeoni, E.; Angeli, V.; Randolph, G. J.; O'Neil, C. P.; Lee, L. K.; Swartz, M. A.; Hubbell, J. A. Exploiting Lymphatic Transport and Complement Activation in Nanoparticle Vaccines. *Nat. Biotechnol.* **2007**, *25*, 1159–1164.
4. Bechet, D.; Couleaud, P.; Frochot, C.; Viriot, M.; Guillemin, F.; Barberi-Heyob, M. Nanoparticles as Vehicles for Delivery of Photodynamic Therapy Agents. *Trends Biotechnol.* **2008**, *26*, 612–621.
5. Ricci-Junior, E.; Marchetti, J. M. Preparation, Characterization, Photocytotoxicity Assay of PLGA Nanoparticles Containing Zinc (II) Phthalocyanine for Photodynamic Therapy Use. *J. Microencapsulation* **2006**, *23*, 523–538.
6. Mönch, I.; Meye, A.; Leonhardt, A. Ferromagnetic Filled Carbon Nanotubes as Novel and Potential Containers for Anticancer Treatment Strategies. In *Nanomaterials for Cancer Therapy; Series Nanotechnologies for the Life Sciences*; Kumar, C. S. S. R., Eds.; Wiley-VCH: 2006; Vol. 6, pp 259−337.
7. Lai, C. W.; Wang, Y. H.; Lai, C. H.; Yang, M. J.; Chen, C. Y.; Chou, P. T.; Chan, C. S.; Chi, Y.; Chen, Y. C.; Hsiao, J. K. Iridium-Complex-Functionalized Fe_3O_4/SiO_2 Core/Shell Nanoparticles: a Facile Three-in-One System in Magnetic Resonance Imaging, Luminescence Imaging, and Photodynamic Therapy. *Small* **2008**, *4*, 218–224.
8. Rodal, G. H.; Rodal, S. K.; Moan, J.; Berg, K. Liposome-Bound Zn(II)-Phthalocyanine. Mechanisms for Cellular Uptake and Photosensitization. *J. Photochem. Photobiol., B* **1998**, *45*, 150–159.

9. Nam, J. M.; Thaxton, C. C.; Mirkin, C. A. Nanoparticles-Based Bio-Barcodes for the Ultrasensitive Detection of Proteins. *Science* **2003**, *301*, 1884–1886.
10. Mahtab, R.; Rogers, J. P.; Murphy, C. J. Protein-Sized Quantum Dot Luminescence Can Distinguish Between "Straight", "Bent", and "Kinked" Oligonucleotides. *J. Am. Chem. Soc.* **1995**, *117*, 9099–9100.
11. Weissleder, R.; Elizondo, G.; Wittenburg, J.; Rabito, C. A.; Bengele, H. H.; Josephson, L. Ultrasmall Superparamagnetic Iron Oxide: Characterisation of a New Class of Contrast Agents for MR Imaging. *Radiology* **1990**, *175*, 489–493.
12. Scherer, F.; Anton, M.; Schillinger, U.; Henke, J.; Bergemann, C.; Krüger, A.; Gänsbacher, B.; Plank, C. Magnetofection: Enhancing and Targeting Gene Delivery by Magnetic Force *in Vitro* and *in Vivo*. *Gene Ther.* **2002**, *9*, 102–109.
13. Robert, D.; Pamme, N.; Conjeaud, H.; Gazeau, F.; Iles, A.; Wilhelm, C. Cell Sorting by Endocytotic Capacity in a Microfluidic Magnetophoresis Device. *Lab Chip* **2011**, *11*, 1902–1910.
14. Megens, M.; Prins, M. Magnetic Biochips: a New Option for Sensitive Diagnostics. *J. Magn. Magn. Mater.* **2005**, *293*, 702–708.
15. Li, G.; Sun, S.; Wilson, R. J.; White, R. L.; Pourmand, N.; Wang, S. X. Spin Valve Sensors for Ultrasensitive Detection of Superparamagnetic Nanoparticles for Biological Applications. *Sens. Actuators A* **2006**, *126*, 98–106.
16. http://www.directindustry.de/industrie-hersteller/microplate-reader-79467.html.
17. Parkin, S. S. P. Giant Magnetoresistance in Magnetic Nanostructures. *Annu. Rev. Mater. Sci.* **1995**, *25*, 357–388.
18. Pannetier, M.; Fermon, C.; Le Goff, G.; Simola, J.; Kerr, E. Femtotesla Magnetic Field Measurement with Magnetoresistive Sensors. *Science* **2004**, *304*, 1648–1650.
19. Hall, D. A.; Gaster, R. S.; Osterfeld, S. J.; Murmann, B.; Wang, S. X. GMR Biosensor Arrays: Correction Techniques for Reproducibility and Enhanced Sensitivity. *Biosens. Bioelectron.* **2010**, *25*, 2177–2181.
20. Shen, W.; Liu, X.; Mazumdar, D.; Xiao, G. *In situ* Detection of Single Micron-Sized Magnetic Beads Using Magnetic Tunnel Junction Sensors. *Appl. Phys. Lett.* **2005**, *86*, 253901.
21. Jiang, Z.; Llandro, J.; Mitrelias, T.; Bland, J. A. C. An Integrated Microfluidic Cell for Detection, Manipulation, and Sorting of Single Micron-Sized Magnetic Beads. *J. Appl. Phys.* **2006**, *99*, 08S105.
22. Schmidt, O. G.; Eberl, K. Thin Solid Films Roll Up into Nanotubes. *Nature* **2001**, *410*, 168.
23. Prinz, V. Y.; Seleznev, V. A.; Gutakovsky, A. K.; Chehovskiy, A. V.; Preobrazenskii, V. V.; Putyato, M. A.; Gavrilova, T. A. Free-Standing and Overgrown InGaAs/GaAs Nanotubes, Nanohelices and Their Arrays. *Phys. E (Amsterdam, Neth.)* **2000**, *6*, 828–831.
24. Kipp, T.; Welsch, H.; Strelow, C.; Heyn, C.; Heitmann, D. Optical Modes in Semiconductor Microtube Ring Resonators. *Phys. Rev. Lett.* **2006**, *96*, 077403.
25. Songmuang, R.; Rastelli, A.; Mendach, S.; Deneke, C.; Schmidt, O. G. From Rolled-Up Si Microtubes to SiOx/Si Optical Ring Resonators. *Microelectron. Eng.* **2007**, *84*, 1427–1430.
26. Huang, G. S.; Mei, Y. F.; Thurmer, D. J.; Coric, E.; Schmidt, O. G. Rolled-Up Transparent Microtubes as Two-Dimensionally Confined Culture Scaffolds of Individual Yeast Cells. *Lab Chip* **2009**, *9*, 263–268.
27. Schulze, S.; Huang, G. S.; Krause, M.; Aubyn, D.; Bolaños Quiñones, V. A.; Schmidt, C. K.; Mei, Y. F.; Schmidt, O. G. Morphological Differentiation of Neurons on Microtopographic Substrates Fabricated by Rolled-Up Nanotechnology. *Adv. Eng. Mater.* **2010**, *12*, B558–B564.
28. Yu, M.; Huang, Y.; Ballweg, J.; Shin, H.; Huang, M.; Savage, D. E.; Lagally, M. G.; Dent, E. W.; Blick, R. H.; Williams, J. C. Semiconductor Nanomembrane Tubes: Three-Dimensional Confinement for Controlled Neurite Outgrowth. *ACS Nano* **2011**, *5*, 2447–2457.
29. Smith, E. J.; Mei, Y. F.; Schmidt, O. G. Optical Components for Lab-in-a-Tube Systems. *Proc. SPIE* **2011**, *8031*, 80310R.
30. Bof Bufon, C. C.; Cojal González, J. D.; Thurmer, D. J.; Grimm, D.; Bauer, M.; Schmidt, O. G. Self-Assembled Ultra-Compact Energy Storage Elements Based on Hybrid Nanomembranes. *Nano Lett.* **2010**, *10*, 2506–2510.
31. Thurmer, D. J.; Bof Bufon, C. C.; Deneke, Ch.; Schmidt, O. G. Nanomembrane-Based Mesoscopic Superconducting Hybrid Junctions. *Nano Lett.* **2010**, *10*, 3704–3709.
32. Ji, H. X.; Wu, X. L.; Fan, L. Z.; Krien, C.; Fiering, I.; Guo, Y. G.; Mei, Y. F.; Schmidt, O. G. Battery Electrodes: Self-Wound Composite Nanomembranes as Electrode Materials for Lithium Ion Batteries. *Adv. Mater.* **2010**, *22*, 4591–4595.
33. Mendach, S.; Songmuang, R.; Kiravittaya, S.; Rastelli, A.; Benyoucef, M.; Schmidt, O. G. Light Emission and Wave Guiding of Quantum Dots in a Tube. *Appl. Phys. Lett.* **2006**, *88*, 111120.
34. Balhorn, F.; Mansfeld, S.; Krohn, A.; Topp, J.; Hansen, W.; Heitmann, D.; Mendach, S. Spin-Wave Interference in Three-Dimensional Rolled-Up Ferromagnetic Microtubes. *Phys. Rev. Lett.* **2010**, *104*, 037205.
35. Smith, E. J.; Makarov, D.; Sanchez, S.; Fomin, V. M.; Schmidt, O. G. Magnetic Micro-Helix Coil Structures. *Phys. Rev. Lett.* **2011**, *107*, 097204.
36. Bermúdez Ureña, E.; Mei, Y. F.; Coric, E.; Makarov, D.; Albrecht, M.; Schmidt, O. G. Fabrication of Ferromagnetic Rolled-Up Microtubes for Magnetic Sensors on Fluids. *J. Phys. D: Appl. Phys.* **2009**, *42*, 055001.
37. Giebeler, C.; Adelerhof, D. J.; Kuiper, A. E. T.; van Zon, J. B. A.; Oelgeschläger, D.; Schulz, G. Robust GMR Sensors for Angle Detection and Rotation Speed Sensing. *Sens. Actuators, A* **2001**, *91*, 16–20.
38. Mei, Y. F.; Solovev, A. A.; Sanchez, S.; Schmidt, O. G. Rolled-Up Nanotech on Polymers: From Basic Perception to Self-Propelled Catalytic Microengines. *Chem. Soc. Rev.* **2011**, *40*, 2109–2119.
39. Mei, Y. F.; Huang, G. S.; Solovev, A. A.; Bermúdez Ureña, E.; Moench, I.; Ding, F.; Reindl, T.; Fu, R. K. Y.; Chu, P. K.; Schmidt, O. G. Versatile Approach for Integrative and Functionalized Tubes by Strain Engineering of Nanomembranes on Polymers. *Adv. Mater.* **2008**, *20*, 4085–4090.
40. Mönch, I.; Schumann, J.; Stockmann, M.; Arndt, K. F.; Schmidt, O. G. Multifunctional Nanomembranes Self-Assembled into Compact Rolled-Up Sensor-Actuator Devices. *Smart Mater. Struct.* **2011**, *20*, 85016.
41. Cendula, P.; Kiravittaya, S.; Mönch, I.; Schumann, J.; Schmidt, O. G. Directional Roll-Up of Nanomembranes Mediated by Wrinkling. *Nano Lett.* **2011**, *11*, 236–240.
42. Lee, R. A.; Donald, D. S. Magtrieve an Efficient, Magnetically Retrievable and Recyclable Oxidant. *Tetrahedron Lett.* **1997**, *38*, 3857–3860.
43. Panuwattanawong, P.; Meiklejohn, W. H.; Kryder, M. H. The Magnetic Moment of CrO_2 Fine Particles. *IEEE Trans. Magn.* **1987**, *23*, 45–47.
44. Stoner, E. C.; Wohlfarth, E. P. A Mechanism of Magnetic Hysteresis in Heterogeneous Alloys. *Philos. Trans. R. Soc., A* **1948**, *240*, 599–642.
45. Baudry, J.; Rouzeau, C.; Goubault, C.; Robic, C.; Cohen-Tannoudji, L.; Koenig, A.; Bertrand, E.; Bibette, J. Acceleration of the Recognition Rate Between Grafted Ligands and Receptors with Magnetic Forces. *Proc. Natl. Acad. Sci. U. S. A.* **2006**, *103*, 16076–16078.
46. Chabert, M.; Viovy, J. L. Microfluidic High-Throughput Encapsulation and Hydrodynamic Self-Sorting of Single Cells. *Proc. Natl. Acad. Sci. U. S. A.* **2008**, *105*, 3191–3196.
47. Harsh, D. C.; Gehrke, S. H. Controlling the Swelling Characteristics of Temperature-Sensitive Celluloseether Hydrogels. *J. Controlled Release* **1991**, *17*, 175–186.